An a priori study of the accuracy of an equilibrium wall model for dissociating air in supersonic channel flows†

By M. Di Renzo AND J. Urzay

1. Motivation and objectives

Numerical simulations of supersonic and hypersonic flows are particularly challenging because of the simultaneous presence of shock waves and turbulence, with transitional zones in compressible boundary layers, and with large fluctuations of temperature, velocity, and pressure (Bertin & Cummings 2006; Leyva 2017; Urzay 2018). In fact, the high kinetic energies that characterize this kind of flows lead to the occurrence of high temperatures in regions where the flow slows down, because of the close coupling between the transfer of momentum and thermal energy. The resulting high temperatures may activate thermochemical processes such as vibrational excitation, dissociation, and ionization (Park 1990; Anderson 2006; Candler 2019).

The intense computational resources required to solve the multiscale dynamics of high-speed flows often forestall the computational analysis of many flow configurations of practical and scientific interest. In this context, the formulation of models able to palliate the computational complexity of the required calculations appears to be a very relevant research topic. For example, a significant effort has been made in this direction with the development of wall models (Kawai & Larsson 2012; Bermejo-Moreno *et al.* 2014; Bae *et al.* 2018; Bose & Park 2018; Iyer & Malik 2019). The present work will discuss an *a priori* assessment of the accuracy of a particular class of wall models, the equilibrium wall models, in high-enthalpy conditions.

The equilibrium wall-models are based on describing the near wall region of the computational domain using the Reynolds-averaged formulation of the transport equations assuming a constant shear layer. A subregion where the wall-model equations are solved is therefore defined within the computational domain of calculation and usually consists of a thin layer spanning the size of the first few grid elements close to the wall. Communication between the near-wall and the outer mathematical formulations happens at the outer end of the wall-model region, which is usually referred as the matching location, where the solution computed using an eddy-resolving formulation is injected to the wall-model problem as a boundary condition, and at the wall, where the shear stress and the heat flux computed using the wall-model equations are used to close the system of equations defined by the outer formulation. Further discussion about the matching between the outer and wall-model problem for high-speed flows is provided by Yang *et al.* (2017). Following this procedure, it is possible to relax the resolution requirements for the near-wall region of the flow, significantly reducing the overall computational cost of the simulation.

† This report is an editorial correction of the original version made on December 23, 2020. Specifically, Eqs. (3.1)-(3.3) were incorrectly typed in the original version and have now been corrected in this version.

The equilibrium wall-model technique, which has been largely validated for flow involving ideal gas, has been recently extended by Muto *et al.* (2019) to multicomponent mixtures in chemical equilibrium. The present study takes another step forward in the process of extending this class of models to the simulation of chemically reacting flows by proposing a formulation of the wall-model equations that takes into account differential diffusion and finite-rate chemistry. The results of the presented formulations are compared with the reference solution of a direct numerical simulation (DNS) performed in a supersonic channel flow with dissociating air. This flow configuration, because of its periodicity in the streamwise and spanwise directions, provides the most favorable conditions to evaluate the accuracy of the wall-model formulation for multiple matching locations.

The brief is organized as follows: the Section 2 defines the transport equations that describe the flow of interest and that are solved in the DNS; the Section 3 provides the formulation of the equilibirum wall-model equations for a multicomponent mixture in chemical non-equilibrium; the setup of the DNS and wall-model calculations discussed in this work is presented in Section 4; the Sec. 5 provides a comparison of the results obtained with the DNS and with the equilibrium wall model focusing on the momentum and energy flux at the wall and on the mean profiles of velocity, temperature, and species molar fractions; and the Section 6 presents conclusions of this work.

2. Transport equations

The DNS presented in this work are performed integrating the compressible Navier-Stokes equations subject to species transport in a chemically reacting mixture of ideal gases, which can be written in compact form as

$$\frac{\partial \mathbf{C}}{\partial t} + \frac{\partial \left[\mathbf{F}(\mathbf{C}) + \mathbf{F}_\nu(\mathbf{C})\right]}{\partial x} + \frac{\partial \left[\mathbf{G}(\mathbf{C}) + \mathbf{G}_\nu(\mathbf{C})\right]}{\partial y} + \frac{\partial \left[\mathbf{H}(\mathbf{C}) + \mathbf{H}_\nu(\mathbf{C})\right]}{\partial z} = \dot{\mathbf{S}} \tag{2.1}$$

in time t and Cartesian coordinates $\{x, y, z\}$. In this formulation, $\mathbf{C}$ is a vector of conserved variables defined as $\mathbf{C} = [\rho_1, \ldots, \rho_{N_s}, \rho u, \rho v, \rho w, \rho e_0]^{\mathrm{T}}$, where the components correspond to the following quantities: (a) the partial densities $\rho_i = \rho Y_i$ of the N_s species in the mixture, with ρ and Y_i being the mixture density and mass fraction of species i, respectively; (b) the three components of the momentum per unit volume ρu, ρv, and ρw, where $\{u, v, w\}$ are the velocity components in the aforementioned Cartesian coordinate system; and (c) the specific stagnation internal energy $e_0 = e + |\mathbf{u}|^2/2$, with e being the specific internal energy of the mixture defined as

$$e = \sum_{i=i}^{N_s} Y_i h_i - P/\rho, \tag{2.2}$$

where P is the thermodynamic pressure and h_i is the partial specific enthalpy of species i given by

$$h_i = h_{i,\mathrm{ref}} + \int_{T_{\mathrm{ref}}}^{T} c_{p,i}(T')dT'. \tag{2.3}$$

The symbol $h_{i,\mathrm{ref}}$ denotes a reference value taken at the reference temperature T_{ref}. In Eq. (2.3), $c_{p,i}$ is the specific heat of species i at constant pressure. These equations are

supplemented with the equation of state

$$P/\rho = \sum_{i=1}^{N_s} Y_i \mathrm{R}^0 T/\mathcal{M}_i \tag{2.4}$$

for an ideal multicomponent gas, where R^0 is the universal gas constant, and $\mathcal{M}_i$ is the molecular weight of species i. In Eq. (2.1), $\mathbf{F}$, $\mathbf{G}$, and $\mathbf{H}$ are Euler fluxes given by

$$\mathbf{F}(\mathbf{C}) = \begin{bmatrix} \rho_1 u \\ \vdots \\ \rho_{N_s} u \\ \rho u u + P \\ \rho u v \\ \rho u w \\ \rho u h_0 \end{bmatrix}, \quad \mathbf{G}(\mathbf{C}) = \begin{bmatrix} \rho_1 v \\ \vdots \\ \rho_{N_s} v \\ \rho v u \\ \rho v v + P \\ \rho v w \\ \rho v h_0 \end{bmatrix}, \quad \mathbf{H}(\mathbf{C}) = \begin{bmatrix} \rho_1 w \\ \vdots \\ \rho_{N_s} w \\ \rho w u \\ \rho w v \\ \rho w w + P \\ \rho w h_0 \end{bmatrix}, \tag{2.5}$$

where $h_0 = e_0 + P/\rho$ is the specific stagnation enthalpy of the mixture. Similarly, $\mathbf{F}_\nu$, $\mathbf{G}_\nu$, and $\mathbf{H}_\nu$ are the diffusion fluxes defined as

$$\mathbf{F}_\nu(\mathbf{C}) = \begin{bmatrix} \rho_1 U_1 \\ \vdots \\ \rho_{N_s} U_{N_s} \\ -\tau_{11} \\ -\tau_{21} \\ -\tau_{31} \\ \displaystyle\sum_{i=1}^{N_s} \rho_i U_i h_i - \lambda \frac{\partial T}{\partial x} - \tau_{11} u - \tau_{12} v - \tau_{13} w \end{bmatrix},$$

$$\mathbf{G}_\nu(\mathbf{C}) = \begin{bmatrix} \rho_1 V_1 \\ \vdots \\ \rho_{N_s} V_{N_s} \\ -\tau_{12} \\ -\tau_{22} \\ -\tau_{32} \\ \displaystyle\sum_{i=1}^{N_s} \rho_i V_i h_i - \lambda \frac{\partial T}{\partial y} - \tau_{21} u - \tau_{22} v - \tau_{23} w \end{bmatrix},$$

and

$$\mathbf{H}_\nu(\mathbf{C}) = \begin{bmatrix} \rho_1 W_1 \\ \vdots \\ \rho_{N_s} W_{N_s} \\ -\tau_{13} \\ -\tau_{23} \\ -\tau_{33} \\ \displaystyle\sum_{i=1}^{N_s} \rho_i W_i h_i - \lambda \frac{\partial T}{\partial z} - \tau_{31} u - \tau_{32} v - \tau_{33} w \end{bmatrix}. \tag{2.6}$$

In these expressions, τ_{ij} $(i,j=1,2,3)$ are the components the viscous stress tensor

$$\overline{\overline{\boldsymbol{\tau}}} = \mu\left[\nabla\mathbf{u} + \nabla\mathbf{u}^T - 2\left(\nabla\cdot\mathbf{u}\right)\overline{\overline{\mathbf{I}}}/3\right], \tag{2.7}$$

where $\overline{\overline{\mathbf{I}}}$ is the identity tensor and μ is the dynamic viscosity of the mixture. Additionally, $\{U_i, V_i, W_i\}$ are the components of the diffusion velocity vector

$$\mathbf{V}_i = -D_i\nabla\left(\ln X_i\right) + \sum_{j=0}^{N_s} Y_j D_j \nabla\left(\ln X_j\right) \tag{2.8}$$

in the Cartesian coordinate system defined above. The right-hand side of Eq. (2.8) for the diffusion velocity is composed of two terms. The first one is a Fickian term, whereas the second one is a mass corrector (Curtiss & Hirschfelder 1949; Coffee & Heimerl 1981; Ern & Giovangigli 1994). In the notation, X_i and D_i are the molar fraction and mass diffusivity of species i, respectively.

The chemical mechanism is formally given by the set of $j = 1, 2, \ldots, M$ elementary steps $\sum_{i=1}^{N_s}\nu'_{ij}\mathcal{R}_i \rightleftharpoons \sum_{i=1}^{N_s}\nu''_{ij}\mathcal{R}_i$, with $\mathcal{R}$ the chemical symbol of species i, ν'_{ij} the stoichiometric coefficient of reactant i in step j on the reactant side, and ν''_{ij} the stoichiometric coefficient of reactant i in step j on the product side. The source term in Eq. (2.1) is defined as $\dot{\mathbf{S}} = \left[\dot{w}_1, \ldots, \dot{w}_{N_s}, 0, 0, 0\right]^T$ in terms of the chemical rates of mass production of species i per unit volume,

$$\dot{w}_i = \mathcal{M}_i\sum_{j=1}^{M}(\nu''_{ij} - \nu'_i)\sum_{i=1}^{N_s}F_{ij}\left(\frac{\rho Y_i}{\mathcal{M}_i}\right)\left[k_{f,j}\prod_{i=1}^{N_s}\left(\frac{\rho Y_i}{\mathcal{M}_i}\right)^{\nu'_{ij}} - k_{b,j}\prod_{i=1}^{N_s}\left(\frac{\rho Y_i}{\mathcal{M}_i}\right)^{\nu''_{ij}}\right], \tag{2.9}$$

where F_{ij} is the chaperon efficiency of species i participating as a collider in reaction j, and $k_{f,j}$ and $k_{b,j}$ are, respectively, the forward and backward rate constants of chemical step j.

Further details about the calculation of the mixture properties, the numerical method, and the solver deployed for the solution of the described transport equations are provided by Di Renzo *et al.* (2019).

3. Equilibrium wall-model equations for a reacting mixture

The formulation of the equilibrium wall model for a chemically reacting flow can be obtained by (a) Favre-averaging the transport equations described in the previous section; (b) imposing the constant shear layer flow conditions, which, taking x and y as the stream-wise and wall-normal directions, read as $\partial/\partial t = 0$, $\partial/\partial x = 0$, and $\partial/\partial z = 0$; and (c) using an eddy-viscosity model to represent the Reynolds stress tensor. The resulting conservation equations for momentum, enthalpy, and species partial density are

$$\frac{d}{dy}\left[\left(\widetilde{\mu}+\mu_t\right)\frac{d\widetilde{u}}{dy}\right] = 0, \tag{3.1}$$

$$\frac{d}{dy}\left[\widetilde{u}\left(\widetilde{\mu}+\mu_t\right)\frac{d\widetilde{u}}{dy} + \widetilde{\lambda}\frac{d\widetilde{T}}{dy} + \frac{\mu_t}{Pr_t}\frac{d\widetilde{h}}{dy} - \sum_{i=1}^{N_s}\widetilde{\rho}_i\widetilde{V}_{y,i}\widetilde{h}_i\right] = 0, \tag{3.2}$$

$$\frac{d}{dy}\left(-\widetilde{\rho}_i\widetilde{V}_i + \frac{\mu_t}{Sc_t}\frac{d\widetilde{Y}_i}{dy}\right) + \widetilde{\dot{w}_i} = 0 \quad \text{for } i = 1, \ldots, N_s, \tag{3.3}$$

where the tilde superscript represents the Favre-averaged quantity. The Favre-averaged mixture properties ($\widetilde{\mu}$, $\widetilde{\lambda}$, $\widetilde{c_p}$, and $\widetilde{D_i}$), wall-normal diffusion velocities ($\widetilde{V}_{y,i}$), and production rates ($\widetilde{\dot{w}_i}$) are evaluated by computing the constitutive relations of the mixture and Eq. (2.8) using the local Favre-averaged mass fractions and temperatures. Two different mixing length models will be deployed in order to estimate the turbulent viscosity. The first, EWM1, estimates μ_t as

$$\mu_t = k\overline{\rho}y\sqrt{\frac{\tau_w}{\overline{\rho}}}\left[1-\exp\left(-\frac{y^+}{A^+}\right)\right]^2, \tag{3.4}$$

where $k = 0.41$ is the von Kármán constant, τ_w is the shear stress at the wall, $y^+ = y/(\nu_w/\sqrt{\tau_w/\rho_w})$ is the dimensionless distance from the wall, ν_w and ρ_w are the kinematic viscosity and the density at the wall, and $A^+ = 17$ is the van Driest damping factor. The second model, EWM2, differs from the first in the way the van Driest damping factor is computed. In this second model, the turbulent viscosity is computed from

$$\mu_t = k\overline{\rho}y\sqrt{\frac{\tau_w}{\overline{\rho}}}\left[1-\exp\left(-\frac{y^*}{A^+}\right)\right]^2, \tag{3.5}$$

where $y^* = y/(\overline{\nu}/\sqrt{\tau_w/\overline{\rho}})$ is the distance from the wall normalized in semi-local units (Huang *et al.* 1995). In the present work, the turbulent Prandtl number Pr_t and the turbulent Schmidt number Sc_t are assumed equal to 0.9.

4. Computational setup

The configuration analyzed in the present study consists of a supersonic channel flow where air, dissociating according to the five species mechanism proposed by Park (1990), flows with a constant mass flux. A uniform pressure gradient is imposed along the streamwise direction in order to keep the flow at a constant bulk Reynolds number $Re_b = \dot{m}_b'' h/\mu_w = 5000$, where $\dot{m}_b''$ is the mass flow rate through the channel per unit cross-sectional area, h is half of the channel height, and μ_w is the dynamic viscosity at the walls of the channel, which are kept at uniform temperature. The compressiblity of the flow is controlled by setting the bulk Mach number $Ma_b = u_b/c_w = 3.0$, where $u_b = \dot{m}_b''/\rho_b$ is the bulk velocity, ρ_b is the bulk density, and c_w is the speed of sound computed at the wall. The walls are assumed to be perfectly non-catalytic $[(\partial Y_i/\partial y)\,|_w = 0]$; consequently, μ_w and c_w are non-linear functions of the local pressure and mixture composition for the considered chemically reacting mixture. For this reason, it is not possible to directly set the desired values of Re_b and Ma_b during the setup of the calculation. It is instead necessary to iteratively rescale the physical dimensions of the channel and the value of $\dot{m}_b''$ in order to reproduce the desired dimensionless configuration. Depending on the initial guess provided to computed the first simulation, this procedure has shown to converge within two or three iterations.

The presence of chemical reactions in the channel introduces additional scales into the problem, making the bulk Reynolds and Mach numbers insufficient to completely identify the computational setup. A bulk Damköhler number is required in order to define the ratio between the fluid dynamic and chemical timescales of the mixture. This dimensionless group is, however, a strongly non-linear function of the bulk thermodynamic state of the mixture, which is part of the solution to the problem. In order to avoid the complex and computationally expensive optimization procedure that would be necessary to set the bulk Damköhler number to a desired value, it has been decided in this study to close

the definition of the computational configuration by setting the values of temperature at the wall and of bulk density inside the channel to $T_w = 1500$ K and $\rho_b = 0.25$ kg/m^3, respectively.

The calculations presented in this work are performed over a computational domain whose dimensions are $8\pi h \times 2h \times 2\pi h$ in the streamwise, wall-normal, and spanwise directions, respectively, and which is discretized using $1024 \times 384 \times 768$ points. The computational grid has a uniform spacing in the streamwise and spanwise directions and an hyperbolic tangent stretching in the wall-normal direction. The stretching parameter of the wall-normal grid distribution function is determined such that it enforces a spacing of the first grid element next to the wall, corresponding to $\Delta y^+ = 0.8$. The dimensions and resolution adopted for the definition of the computational grid have been shown to be sufficient to fully resolve similar channel-flow configurations already discussed in the literature (Sciacovelli *et al.* 2017; Di Renzo *et al.* 2019). The flow is initialized with constant pressure, temperature, and composition ($X_{N_2} = 0.79$ and $X_{O_2} = 0.21$) along with an axial velocity profile that is a function of the fourth power of the wall-normal distance and guarantees the expected mass flux $\dot{m}_b''$. Counter-rotating vortices whose axis is aligned with the stream-wise direction are superposed on this initial condition. The flow evolves until the bulk temperature and pressure in the domain reach a statistically steady state. Time averages are then collected over a time interval of order $3000\nu_w/u_\tau^2$, where $u_\tau = \sqrt{\tau_w/\rho_w}$ is the friction velocity.

The performance of the two wall models is evaluated using four different hypothetical matching locations, namely, $y_m^+ = 15$, 50, 100, and 150. In particular, the Favre-averaged thermodynamic state and the streamwise velocity of the mixture obtained from the DNS calculation are set as the outer boundary conditions for the wall-model equations, which are discretized on a stretched grid of 150 points using second-order central finite differences. The resulting non-linear system of equations is integrated using a Newton method modified with a line-search algorithm in order to increase the convergence rate. A tolerance of 10^{-12} is used in order to check the convergence of the solution.

5. Results

This section compares the results obtained by Favre-averaging the results of the DNS simulation and the solution of the equilibrium wall-model equations. The comparison starts by analyzing the values of the shear stress (expressed in terms of $Re_\tau = \rho_w u_\tau h/\mu_w$) and of the dimensionless heat flux at the wall $B_q = q_w/(\rho_w u_\tau c_{p,w} T_w)$, where $c_{p,w}$ is the mixture-averaged constant-pressure heat capacity at the wall. These energy and momentum fluxes are the main outcome of the equilibrium wall-model formulation when it is deployed as a boundary condition; therefore, matching these quantities is a necessary condition to ensure its accuracy. However, it is noteworthy that the present *a priori* analysis neglects all the non-linear interactions that are present between the wall model and the outer formulation of the problem, making the following comparison insufficient to completely assess the accuracy of the model. The values of the fluxes predicted by the three different formulations and for the four matching locations are reported in Table 1. On the one hand, the predictions of the EWM1 formulation show a moderate error (order 5%) when the matching location is imposed at $y_m^+ = 15$. However, the error rapidly increases to about 30% for both the Re_τ and the dimensionless heat flux as soon as the matching location is moved to $y_m^+ = 50$. Interestingly, the error with respect to the DNS is similar for the three matching locations with $y_m^+ \leq 50$, suggesting that the EWM1

		$y_m^+ = 15$		$y_m^+ = 50$		$y_m^+ = 100$		$y_m^+ = 150$	
	DNS	EWM1	EWM2	EWM1	EWM2	EWM1	EWM2	EWM1	EWM2
Re_τ	438.2	466.8	434.9	557.3	448.8	554.2	441.8	544.9	437.8
$B_q \times 10^3$	117.5	122.8	115.6	153.2	124.3	156.1	125.3	154.5	125.1

TABLE 1. Reynolds number based on friction units and dimensionless heat flux at the wall computed using the DNS and the equilibrium wall-model formulations for different matching locations.

introduces modelling errors in the region $15 \leq y_m^+ \leq 50$ that invalidate the accuracy of all the wall-model solutions in domains that cross this region. On the other hand, the EWM2 is able to predict values of Re_τ and B_q that are within a 5% error with respect to the DNS results, demonstrating a better accuracy of the mixing length model when it is applied in the semi-local units.

Further details about the source of the mismatch between the wall-model formulations and the DNS can be found by analyzing the distribution of streamwise velocity, of temperature, and of the atomic oxygen molar fraction. The first two quantities are the main drivers of the momentum and energy fluxes reported in Table 1. The molar fraction of atomic oxygen is, in contrast, a good proxy for assessing the errors introduced by the Favre-averaging of the wall-model equations on the the prediction of the chemical dissociation inside the boundary layer.

Figure 1 shows the streamwise velocity profiles obtained for the four analyzed matching locations. Each solid line corresponds to the solution obtained with the DNS, whereas the lines with symbols correspond to the solutions of the two equilibrium wall-model formulations. Note that the friction units computed with the DNS have been retained to normalize the quantities in the graph in order to ease the comparison between the shapes of the obtained profiles. Consistent with the observation made regarding the values in Table 1, both of the solutions obtained with EWM1 and EWM2 for $y_m^+ = 15$ are in good agreement with the results of the DNS, as shown in Figure 1(a). When the matching location in positioned at $y_m^+ \geq 50$, the EWM1 formulation loses its accuracy with respect to the DNS solution. In particular, it predicts a transition location between the logarithmic and linear scaling of the velocity profile, which is positioned closer to the wall than in the reference profile. The position of this buffer layer remains constant for the three matching locations that are positioned further away from the wall, suggesting that this particular shape of the velocity profile is embedded in the mixing length model deployed in the calculations. The similar slope of the logarithmic scaling that is observed for the wall-model and DNS solutions suggests that the weakest link in Eq. (3.4) is the van Driest damping that triggers the transition from the linear to the logarithmic scaling of the profile. This hypothesis is also corroborated by the very good agreement observed for the EWM2 at all the matching locations.

Figure 2 compares of the profiles of Favre-averaged temperature for the DNS and the wall-model calculations. The discrepancies observed for the velocity profiles are similar to those for the temperature distributions. The EWM1 formulation with a matching location $y_m^+ \geq 50$ predicts a thinner thermal boundary layer that triggers a stronger heat flux at the wall. However, in this case the evaluation of the van Driest damping factor using the semi-local units is only able to partially mitigate the modelling error introduced

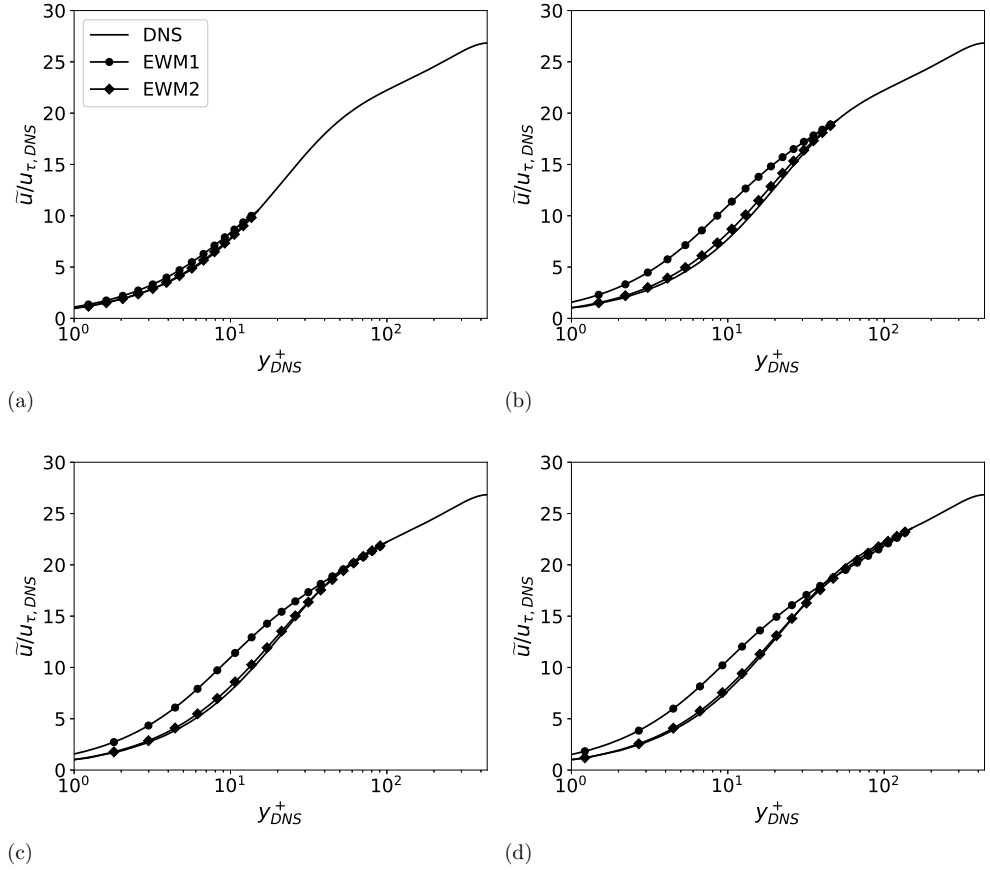

FIGURE 1. Comparison of the Favre-averaged streamwise velocity profiles obtained with the DNS and the equilibrium wall-model calculations for a matching location (a) $y_m^+ = 15$, (b) $y_m^+ = 50$, (c) $y_m^+ = 100$, and (d) $y_m^+ = 150$.

by the evaluation of the turbulent heat conductivity with the mixing length model. In fact, the thermal boundary layer thickness computed with the EWM2 formulation does not collapse on the DNS results but still provides the best estimation of the temperature distribution in the channel.

A comparison of the distribution of the atomic oxygen molar mass is presented in Figure 3. This quantity shows the worst agreement with respect to the DNS results, with the wall-model formulations predicting a significantly higher concentration of the atomic oxygen for all matching locations. A possible source of this modelling error could be the higher temperatures observed in the wall-model solutions, which increase the average dissociation rate of the mixture. However, the Figure 3(a) suggests that the modelling errors are only partially related to the higher temperatures. In fact, the wall-model calculations performed with $y_m^+ = 15$ predict a temperature profile which is very similar to the DNS results but still with computed oxygen molar fraction profiles that are significantly different from those of the reference solution. For this reason, it is possible to postulate that the most relevant source of error in the wall-model formulation is related to the computation of the Favre-averaged chemical production rates. In particular, the assumption $\widetilde{\dot{w}_i} = \dot{w}_i(\widetilde{Y}_i, \widetilde{T}, P)$, which is required for the formulation of the wall-model

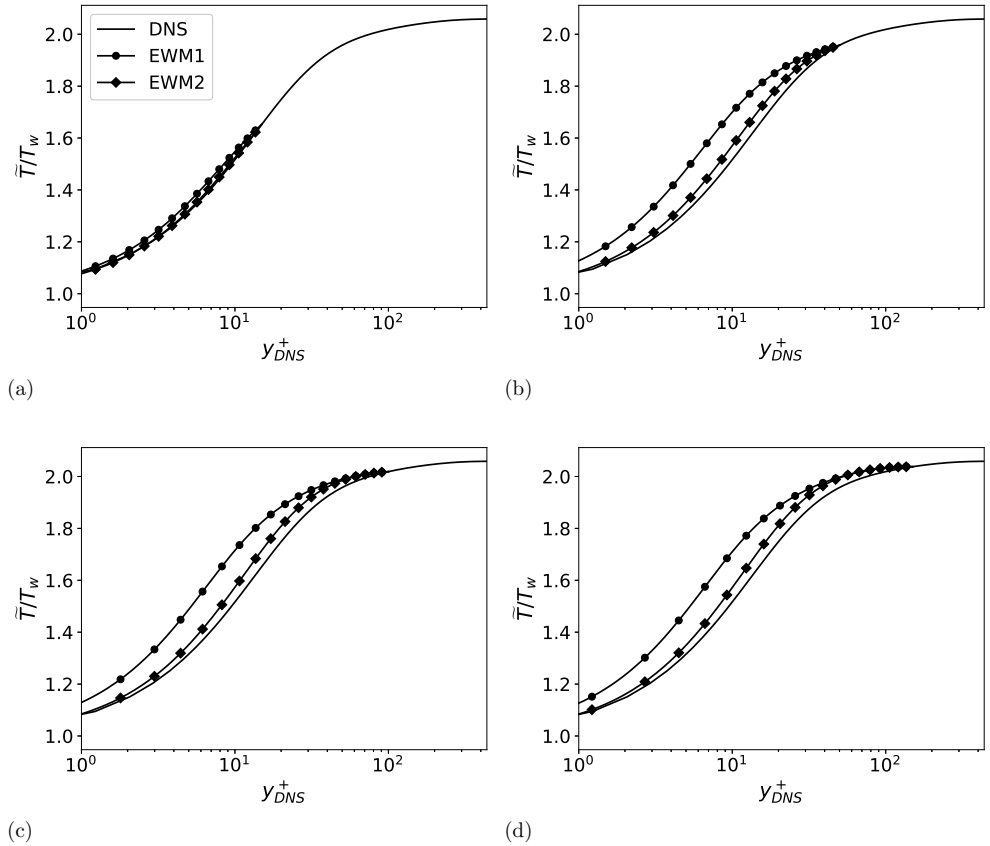

FIGURE 2. Comparison of the Favre-averaged temperature profiles obtained with the DNS and the equilibrium wall-model calculations for a matching location (a) $y_m^+ = 15$, (b) $y_m^+ = 50$, (c) $y_m^+ = 100$, and (d) $y_m^+ = 150$.

equations, can lead to very large errors, because the function that relates the production rates to the local thermochemical condition of the mixture is strongly non-linear and applying it directly to the Favre-averaged quantities neglects the intermittency of the thermochemical state of the mixture in the boundary layer. This is a well-known issue in the combustion community, and multiple approaches have been developed to overcome it (Peters 2004; Pierce & Moin 2004; Ihme & Pitsch 2008*a*,*b*). However, an assessment of the accuracy of these methods in the context of wall modeling is still required and will be part of future investigations.

6. Conclusions

This study presents an *a priori* study of the accuracy of equilibrium wall models in a supersonic reacting channel flow. A turbulent channel flow with bulk Mach number equal to three and bulk Reynolds number equal to 5000 has first been solved using a DNS including the effects of air chemical dissociation on the composition of the computed ideal gas mixture. The accuracy of two formulations for the equilibrium wall-model equations, which differ in the evaluation of the van Driest damping factor, has been tested, taking the Favre-averaged solution of the direct simulation as a reference. The wall-model formu-

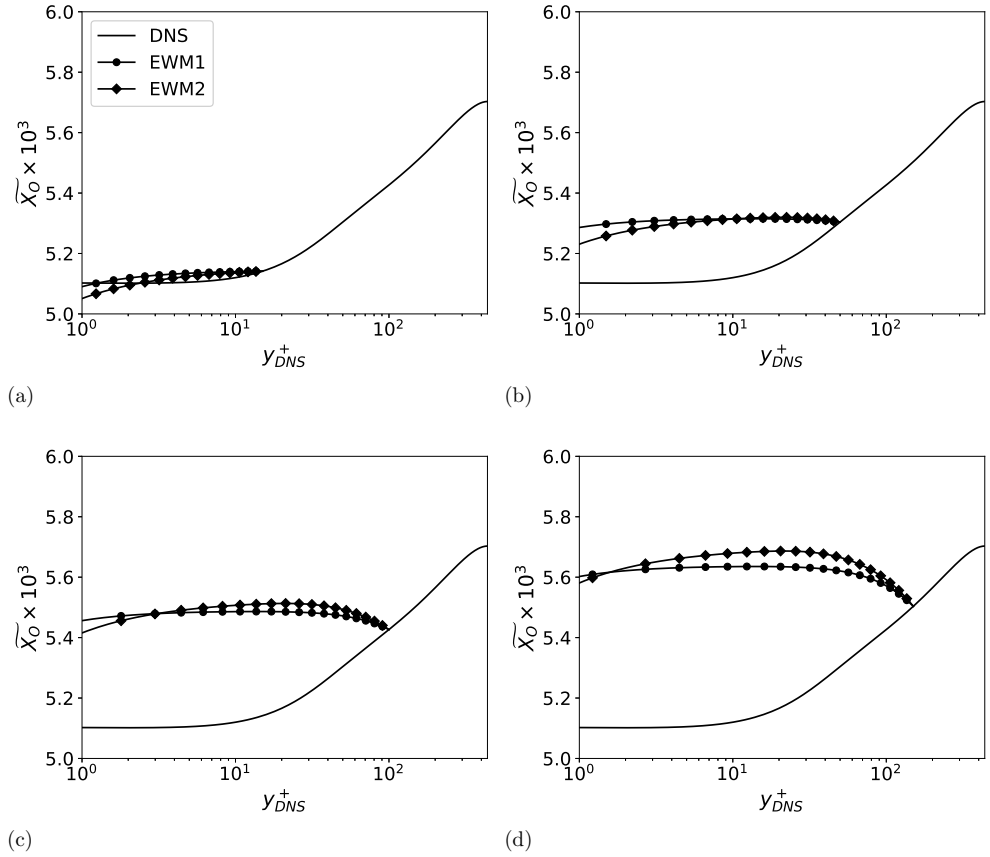

FIGURE 3. Comparison of the Favre-averaged atomic oxygen molar fraction profiles obtained with the DNS and the equilibrium wall-model calculations for a matching location (a) $y_m^+ = 15$, (b) $y_m^+ = 50$, (c) $y_m^+ = 100$, and (d) $y_m^+ = 150$.

lation based on the semi-local scaling of the wall-normal distance for the evaluation of the turbulent viscosity has been shown to produce better predictions of the fluxes at the wall and of mean velocity and temperature profiles. Both the wall-model formulations tested in this work fail to predict the correct profile of oxygen molar fraction in the mixture. The approximation that computes the chemical production rate from the Favre-averaged mass fractions and temperature is deemed to be the main source of error leading to this discrepancy and calls for additional studies on this aspect of the wall-model formulation.

Acknowledgments

This investigation is funded by the U.S. Air Force Office of Scientific Research (AFOSR), grant # 1194592-1-TAAHO, and by the Advanced Simulation and Computing (ASC) program of the U.S. Department of Energy's National Nuclear Security Administration (NNSA) via the PSAAP-II Center at Stanford, grant # DE-NA0002373. The authors thank Adrián Lozano-Durán for his critical review of this manuscript.

REFERENCES

Anderson, J. D. J. 2006 *Hypersonic and High-Temperature Gas Dynamics*. AIAA.

Bae, H. J., Lozano-Durán, A., Bose, S. T. & Moin, P. 2018 Dynamic slip wall model for large-eddy simulation. *J. Fluid Mech.* **859**, 400–432.

Bermejo-Moreno, I., Larsson, J. & Bodart, J. 2014 Wall modeled large-eddy simulation of shock wave/turbulent boundary layer interaction with separation. *Annual Research Briefs*, Center for Turbulence Research, Stanford University, pp. 155–167.

Bertin, J. J. & Cummings, R. M. 2006 Critical hypersonic aerothermodynamic phenomena. *Annu. Rev. Fluid Mech.* **38**, 129–157.

Bose, S. T. & Park, G. I. 2018 Wall-Modeled large-Eddy simulation for complex turbulent flows. *Annu. Rev. Fluid Mech.* **50**, 535–561.

Candler, G. V. 2019 Rate effects in hypersonic flows. *Annu. Rev. Fluid Mech.* **51**, 379–402.

Coffee, T. P. & Heimerl, J. M. 1981 Transport algorithms for premixed, laminar steady-state flames. *Combust. Flame* **43**, 273–289.

Curtiss, C. F. & Hirschfelder, J. O. 1949 Transport properties of multicomponent gas mixtures. *J. Chem. Phys.* **17**, 550–555.

Di Renzo, M., Fu, L. & Urzay, J. 2019 HTR solver: An open-source exascale-oriented task-based multi-GPU high-order code for hypersonic aerothermodynamics. *Submitted for publication*.

Ern, A. & Giovangigli, V. 1994 *Multicomponent Transport Algorithms*, *Lect. Notes Phys. Monographs*, vol. 24. Springer.

Huang, P. G., Coleman, G. N. & Bradshaw, P. 1995 Compressible turbulent channel flows: DNS results and modelling. *J. Fluid Mech.* **305**, 185–218.

Ihme, M. & Pitsch, H. 2008*a* Prediction of extinction and reignition in nonpremixed turbulent flames using a flamelet/progress variable model 1. A priori study and presumed PDF closure. *Combust. Flame* **155**, 80–89.

Ihme, M. & Pitsch, H. 2008*b* Prediction of extinction and reignition in nonpremixed turbulent flames using a flamelet/progress variable model 2. Application in LES of Sandia flames D and E. *Combust. Flame* **155**, 90–107.

Iyer, P. & Malik, M. 2019 Analysis of the equilibrium wall model for high-speed turbulent flows. *Phys. Rev. Fluids* **4**, 074604.

Kawai, S. & Larsson, J. 2012 Wall-modeling in large eddy simulation: Length scales, grid resolution, and accuracy. *Phys. Fluids* **24**, 015105.

Leyva, I. A. 2017 The relentless pursuit of hypersonic flight. *Phys. Today* **70**, 30–36.

Muto, D., Daimon, Y., Shimizu, T. & Negishi, H. 2019 An equilibrium wall model for reacting turbulent flows with heat transfer. *Int. J. Heat Mass Tran.* **141**, 1187–1195.

Park, C. 1990 *Nonequilibrium Hypersonic Aerothermodynamics*. Wiley.

Peters, N. 2004 *Turbulent Combustion*. Cambridge University Press.

Pierce, C. D. & Moin, P. 2004 Progress-variable approach for large-eddy simulation of non-premixed turbulent combustion. *J. Fluid Mech.* **504**, 73–97.

Sciacovelli, L., Cinnella, P., & Gloerfelt, X. 2017 Direct numerical simulations of supersonic turbulent channel flows of dense gases. *J. Fluid Mech.* **821**, 153–199.

Urzay, J. 2018 Supersonic combustion in air-breathing propulsion systems for hypersonic flight. *Annu. Rev. Fluid Mech.* **50**, 593–627.

Yang, X. I. A., Urzay, J., Bose, S. T. & Moin, P. 2017 Aerodynamic heating in wall-modeled large-eddy simulation of high-speed flows. *AIAA J.* **56**, 731-742.